Journal of Power Sources 188 (2009) 483–488

Contents lists available at ScienceDirect

Journal of Power Sources

journal homepage: www.elsevier.com/locate/jpowsour

Stable, easily sintered Ca–Zn-doped $YCrO_3$ as novel interconnect materials for co-fired yttrium-stabilized zirconia-based solid oxide fuel cells

Songlin Wang[a], Bin Lin[a], Yingchao Dong[a,b], Daru Fang[a], Hanping Ding[a], Xingqin Liu[a,*], Guangyao Meng[a]

[a] Department of Materials Science and Engineering, University of Science and Technology of China (USTC), Hefei, Anhui 230026, PR China
[b] University Key Laboratory for Inorganic Membrane in Jiangxi Province, National Engineering Research Center for Domestic and Building Ceramics, Jingdezhen Ceramic Institute (JCI), Jingdezhen, Jiangxi 333001, PR China

ARTICLE INFO

Article history:
Received 28 November 2008
Accepted 2 December 2008
Available online 7 December 2008

Keywords:
Yttrium chromite
Sintering ability
Sol–gel process
Interconnect
SOFC

ABSTRACT

In order to develop co-fired yttrium-stabilized zirconia (YSZ)-based solid oxide fuel cells (SOFCs), stable and easily sintered $Y_{0.7}Ca_{0.3}Cr_{1-x}Zn_xO_{3-\delta}$ ($x = 0$–0.15) perovskite oxides were synthesized by the microwave-aided sol–gel process and then examined as novel ceramic interconnect materials. (The characterizations focused on phase structure, sintering behavior, relative density, electrical conductivity and thermal expansion.) The XRD analysis indicates that a pure orthorhombic perovskite phase was obtained for all the samples. Cell volume decreases as x increases from 0 to 0.10. The $Y_{0.7}Ca_{0.3}Cr_{0.9}Zn_{0.1}O_{3-\delta}$ (YCCZ10) powder exhibited the best sintering ability, and a relative density of 96.6% could be obtained for the sample sintered at 1400 °C for 4 h in air. The electrical conductivities of the specimens increase with the Zn^{2+} content at $x \leq 0.10$, but then remarkably decrease at $x = 0.15$, which might relate to the over-range of the substitution amount of Zn (0.15) for Cr position. YCCZ10 shows a remarkable electrical conductivity of 20.9 S cm^{-1} at 850 °C in air, and a very suitable thermal expansion coefficient value of 10.8×10^{-6} K^{-1} (YSZ: $\sim 10.8 \times 10^{-6}$ K^{-1}). These investigations have indicated that YCCZ10 is a promising interconnect material for co-fired YSZ-based SOFCs.

1. Introduction

Solid oxide fuel cells (SOFCs) now have attracted more and more attention worldwide due to their high efficiency and low pollution [1,2]. Great progresses have been made on the research of individual cells, such as high performance and cost-effective manufacture processes. While some material challenges still exist, which hold back individual fuel cells from being compiled into stacks. Interconnect, serving as an electrical contact between individual cells in SOFC stack, is currently becoming a crucial issue for the development of SOFCs. For a good interconnect material at fuel cell operating or fabricating conditions, a number of specific requirements are to be met, just shown as follows: (a) high electronic conductivity, (b) negligible ionic conductivity, (c) high chemical stability under a wide range of oxygen potential at high temperatures, (d) matched thermal expansion with other cell components, especially with electrolyte, (e) gas tightness, and (f) high mechanical strength. These rigorous requirements eliminate all but only a few oxide systems from consideration for SOFC interconnect, among which the most promising material is $LaCrO_3$ and $YCrO_3$ system [3–7]. High-temperature alloys have also been considered as interconnect materials, but which are only used for flat-plate SOFCs operated below 800 °C.

Currently, $LaCrO_3$ system has attracted much more attention and encouraging breakthroughs have been achieved using various approaches in order to improve its properties, such as sintering ability and electrical conductivity [8–11]. However, to the best of our knowledge, it has not been reported so far that dense ceramic interconnect membrane is made on porous anode support by the cost-effective co-firing process. $LaCrO_3$ is chemically stable with state-of-the-art YSZ electrolyte below 1300 °C. At higher temperatures, however, the reaction between them results in the production of $La_2Zr_2O_7$ phase with high resistance, which prohibits the application of $LaCrO_3$ system [12,13]. This is one reason why it is quite difficult to prepare dense $LaCrO_3$-based interconnect membrane on NiO/YSZ anode by co-firing. By contrast, $YCrO_3$ is more stable in SOFC operating conditions, though the melting point of $YCrO_3$ is lower than that of $LaCrO_3$ [14]. Furthermore, no chemical reaction can occur, and therefore other impure phases can be effectively avoided at co-firing temperatures (usually 1400 °C) when $YCrO_3$ system is chosen as interconnect material. However, to date, only a few studies have focused on the properties of yttrium

* Corresponding author. Tel.: +86 551 3606249; fax: +86 551 3607627.
E-mail address: xqliu@ustc.edu.cn (X. Liu).

0378-7753/$ – see front matter © 2008 Elsevier B.V. All rights reserved.
doi:10.1016/j.jpowsour.2008.12.005

chromite system [6,15–17], and little is known regarding how to densely sinter this kind of material at a cell co-firing temperature in air.

In this work, novel interconnect materials of $Y_{0.7}Ca_{0.3}Cr_{1-x}Zn_xO_{3-\delta}$ (x = 0–0.15) were synthesized by a microwave-aided sol–gel process. The sintering character, crystalline phase structure, electrical conductivity and thermal expansion coefficient of $Y_{0.7}Ca_{0.3}Cr_{1-x}Zn_xO_{3-\delta}$ were investigated as a function of Zn content in detail.

2. Experimental

The fine powders of $Y_{0.7}Ca_{0.3}Cr_{1-x}ZnO_{3-\delta}$ (x = 0, 0.05, 0.10, 0.15) were, respectively, synthesized by a microwave-aided sol–gel process with stoichiometric precursors of yttrium oxide (Y_2O_3), calcium nitrate ($Ca(NO_3)_2{\cdot}4H_2O$), chromic nitrate ($Cr(NO_3)_3{\cdot}9H_2O$), and zinc nitrate ($Zn(NO_3)_2{\cdot}6H_2O$) (all analytical reagents, Sinopharm Chemical Reagent Co., Ltd.), mixing together with three times as much citric acid in deionized water. The mixture was heated up in a crucible to form a gel. Afterwards, the wet gel was further heated in a family-using microwave oven to remove solvents and to obtain dry gel. Then, mild combustion reaction took place, and the dark precursor powders were formed. The as-synthesized powders were calcined at 850 °C for 2 h to remove the remnant carbon and to obtain the highly reactive fine powders.

The as-synthesized powders were ball-milled in an ethanol medium for 24 h and dried subsequently. Small pellets (Ø15 mm × 0.8 mm) and rectangular bar specimens (50 mm × 5 mm × 1.8 mm) were uniaxially pressed at 360 MPa. The specimens were sintered in air at 1400 °C for 4 h. The heating rate was fixed at 1 °C min^{-1} before 550 °C and 2 °C min^{-1} between 550 °C and 1400 °C.

Thermogravimetry (TG) of the dry gel (by PerkinElmer Diamond TG/DTA) was carried out in air from room temperature to 1100 °C with a heating rate of 10 °C min^{-1}. $Y_{0.7}Ca_{0.3}Cr_{1-x}Zn_xO_{3-\delta}$ powders were observed using a high-resolution transmission electron microscope (HR-TEM, Model JEOL-2010). X-ray diffraction (XRD) patterns of the primary powders and sintered specimens were respectively measured with a XRD instrument (Philips, PW 1730) powered at 40 kV and 100 mA using Cu Kα radiation in air at room temperature. The diffraction intensity was measured stepwise every 0.02° in the diffraction angle 2θ range between 20° and 80°. The relative densities were measured by the Archimedes method. Theoretical densities were calculated using experimental lattice parameters and chemical formula $Y_{0.7}Ca_{0.3}Cr_{1-x}Zn_xO_{3-\delta}$. Particle size and fractured surfaces of the sintered specimens were observed using a scanning electron microscopy (SEM, Model KYKY 1010B). Electrical conductivities of the materials in air were studied from 500 °C to 850 °C using a standard DC four-probe technique on a H.P. multimeter (Model 34401). Sintering shrinkage of the green pellets and thermal expansion of the sintered specimens were measured at 30–1400 °C and 30–1000 °C, respectively, on cylindrical rods using a dilatometer (SHIMADZU50) at a heating rate of 10 °C min^{-1}.

3. Results and discussion

3.1. Powder characterization

The powders of $Y_{0.7}Ca_{0.3}Cr_{1-x}Zn_xO_{3-\delta}$ (x = 0, 0.05, 0.1, 0.15) were, respectively, synthesized via the microwave-aided sol–gel process. The dry gel was characterized by TG in order to understand physicochemical transitions at different temperatures. The TG curve of the YCCZ10 dry gel is shown in Fig. 1, which shows three stages of weight loss. The first weight loss with 13.3% takes place below

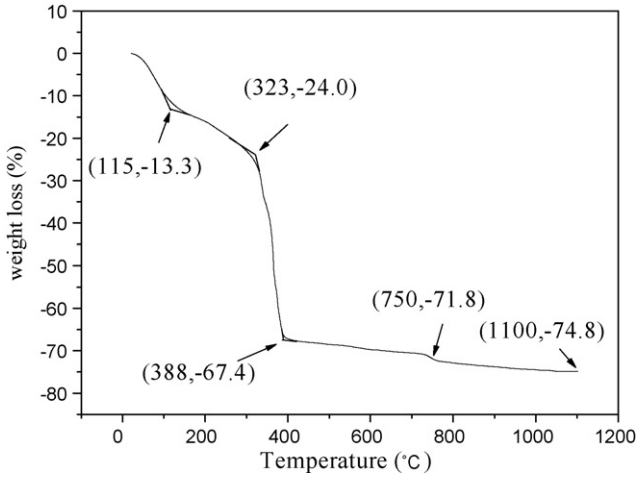

Fig. 1. TG analysis of YCCZ10 precursor powders (heating rate 10 °C min^{-1}).

115 °C. This is due to the evaporation of surface adsorbed water molecules. With temperature further increasing, the 10% weight loss of structure and crystallization water occurs, which relate to the second stage from 115 °C to 323 °C. The largest weight loss of 43.4% happens at the third stage from 323 °C to 388 °C, which attributes to the combustion of the mixed citric acid and nitrate. In this period, metal cations and carbon element of citric acid are oxidized and nitrate is reduced. The fourth small weight loss occurs from 388 °C to 750 °C. This is caused by the removal of the remnant nitrate and carbon.

There is a slight weight loss of about 1.5% at 750 °C, which is ascribed to the formation of perovskite $CaCrO_3$ via the decomposition of second phase $CaCrO_4$ in air at high temperature:

$$2CaCrO_4 = 2CaCrO_3 + O_2 \quad (1)$$

Therefore, the calcination temperature of the precursor powders should be above 750 °C.

Fig. 2 shows the HR-TEM micro-photographs of the $Y_{0.7}Ca_{0.3}Cr_{1-x}Zn_xO_{3-\delta}$ (x = 0, 0.05, 0.1) powders calcined at 850 °C for 2 h. As Zn doping amount increases, the particle size increases and its distribution becomes gradually broaden. The particle diameters are in the ranges of 30–100 nm for x = 0, 40–200 nm for x = 0.05, and 50–500 nm for x = 0.1, respectively. The YCCZ10 consists of fine particles with a relatively wider size distribution, indicating the partial agglomeration of particles at 850 °C. The powder with wide size distribution (particle gradation) is expected to have a high sintering activity because of its high packing density. This is effectively verified by the sintering characteristic of the powder.

Fig. 3 shows the sintering shrinkage behavior of the green pellets of $Y_{0.7}Ca_{0.3}Cr_{1-x}Zn_xO_{3-\delta}$ (x = 0, 0.05, 0.10) measured at 30–1400 °C. It is obvious that there is almost no shrinkage for all the pellets below 950 °C. Above that temperature, the shrinkage curve of YCCZ10 presents a long step region between 1000 °C and 1100 °C and large shrinkage happens rapidly after the flat region, while $Y_{0.7}Ca_{0.3}CrO_{3-\delta}$ does not show such a flat region. The sample of $Y_{0.7}Ca_{0.3}Cr_{0.95}Zn_{0.05}O_{3-\delta}$ shows moderate shrinkage behaviour between $Y_{0.7}Ca_{0.3}CrO_{3-\delta}$ and YCCZ10. It can be predicted that the doped Zn as sintering aid may happen at a certain temperature range of 1000–1100 °C, thus the shrinkage curve shows a flat region at that temperature. At 1400 °C, the shrinkage ratio (dL/L_0) increases from 9.6% to the maximum of 22% as the x value increases from 0 to 0.1. The results indicate that Zn doping can effectively improve the sintering ability of the material, and that the YCCZ10 with 10% Zn doping exhibits the most sintering activity.

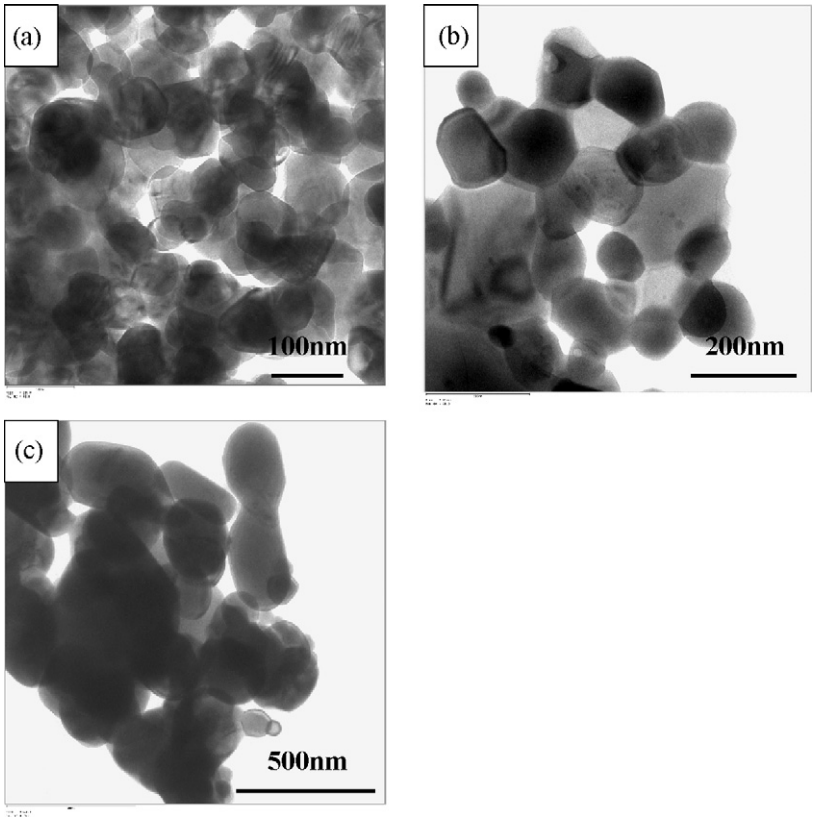

Fig. 2. HR-TEM micro-photographs of $Y_{0.7}Ca_{0.3}Cr_{1-x}Zn_xO_{3-\delta}$ powders calcined at 850 °C for 2 h: (a) $Y_{0.7}Ca_{0.3}CrO_{3-\delta}$; (b) $Y_{0.7}Ca_{0.3}Cr_{0.95}Zn_{0.05}O_{3-\delta}$; (c) YCCZ10.

3.2. XRD phase structure analysis

The XRD patterns of the sintered samples (1400 °C for 4 h) of the system $Y_{0.7}Ca_{0.3}Cr_{1-x}Zn_xO_{3-\delta}$ (x = 0, 0.05, 0.10, and 0.15) are shown in Fig. 4. The XRD patterns of the compositions in the range of x = 0–0.15 all show single phase with orthorhombic perovskite structure. The peaks corresponding to plane (0 2 1) become gradually lower with x value increasing from 0 to 0.1, and then not obvious at x = 0.15, which relates to the lattice distortion induced by the substitution of Zn atom for Cr position. From Table 1, it is apparent that

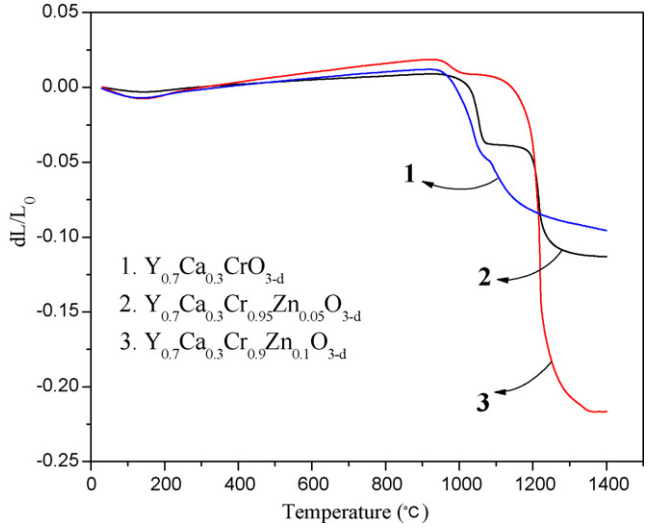

Fig. 3. Sintering shrinkage of the pellet of $Y_{0.7}Ca_{0.3}Cr_{1-x}Zn_xO_{3-\delta}$ pressed using the primary powder calcined at 850 °C for 2 h.

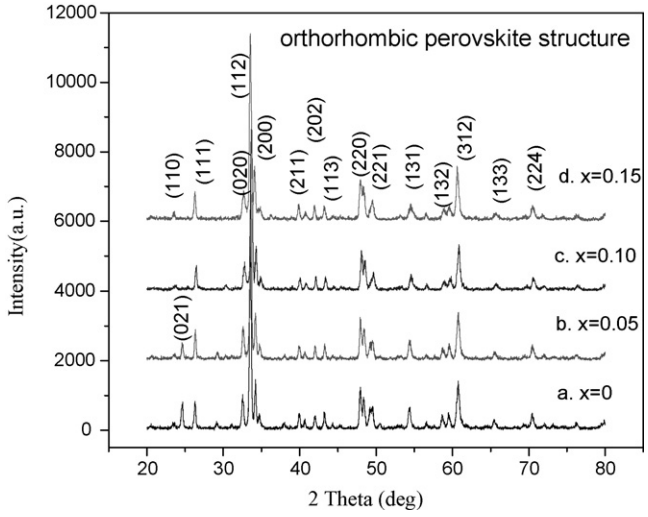

Fig. 4. XRD patterns of $Y_{0.7}Ca_{0.3}Cr_{1-x}Zn_xO_{3-\delta}$ sintered at 1400 °C for 4 h.

Table 1
Characteristics of $Y_{0.7}Ca_{0.3}Cr_{1-x}Zn_xO_{3-\delta}$ sintered at 1400 °C for 4 h.

	x value			
	0	0.05	0.10	0.15
a (nm)	0.5237	0.5228	0.5227	0.5245
b (nm)	0.5496	0.5484	0.5459	0.5479
c (nm)	0.7518	0.7522	0.7485	0.7534
Cell volume (nm^3)	0.2164	0.2156	0.2136	0.2165
Relative density (%)	84.3	90.2	96.6	95.3
Electrical conductivity at 750 °C ($S\,cm^{-1}$)	1.9	5.9	19.0	11.5
Activate energy (kJ/mol)	17.5	17.3	17.9	21.3
TEC ($\times 10^{-6}\,K^{-1}$)	9.6	10.0	10.8	9.3

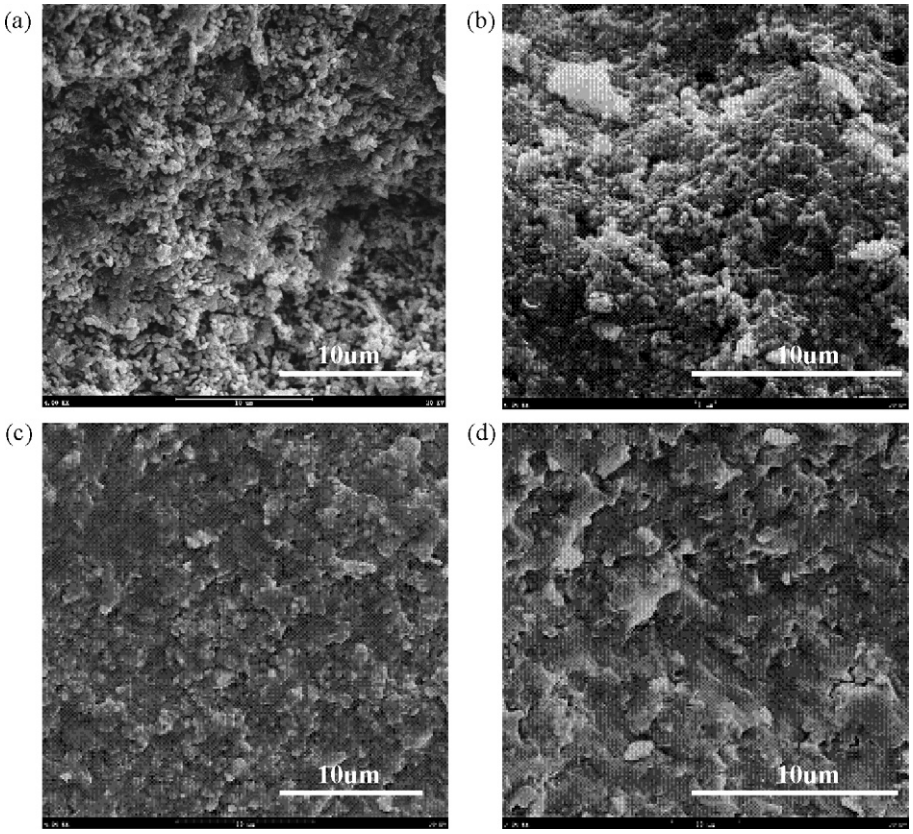

Fig. 5. SEM micrographs for fracture surfaces of $Y_{0.7}Ca_{0.3}Cr_{1-x}Zn_xO_{3-\delta}$ sintered at 1400 °C for 4 h: (a) $x = 0$; (b) $x = 0.05$; (c) $x = 0.10$; (d) $x = 0.15$.

the unit cell lattice parameter of $Y_{0.7}Ca_{0.3}Cr_{1-x}Zn_xO_{3-\delta}$ (calculated from the XRD results) changes with x value variety. It can be seen that the cell volume decreases from 0.2164 nm^3 to 0.2136 nm^3 as x increases from 0 to 0.10. The increasing substitution of Zn^{2+} for Cr^{3+} leads to the decreasing of cell volume. This is not only because of the smaller radius of Zn^{2+} (0.060 nm) than Cr^{3+} (0.064 nm), but also for the increased concentration of Cr^{4+} (0.056 nm). Using the Kroger–Vink notation, it can be descried as

$$[Ca_Y'] + [Zn_{Cr}'] = 2[V_O^{\bullet\bullet}] + [Cr_{Cr}^{\bullet}] \quad (2)$$

where [] indicates concentration, Ca_Y' *is* Ca^{2+} substituted for Y^{3+}, Zn_{Cr}' is Zn^{2+} on Cr-site, $V_O^{\bullet\bullet}$ means oxygen vacancy, and $Cr_{Cr}^{\bullet}$ is Cr^{4+} on Cr-site. The smaller Cr^{4+} ions (0.056 nm) decrease the volume of the unit cell.

However, with x further increasing up to 0.15, the calculated cell volume increases to 0.2165 nm^3, indicating that the amount of Zn may exceeds the substitution limit for Cr position (between 0.10 and 0.15). And the excessive Zn atom might partly come into the perovskite crystal interstitial position, resulting in the increasing in cell volume.

3.3. Relative density measurements and SEM analysis

The relative densities of the samples sintered at 1400 °C for 4 h in air are shown in Table 1. As the doping amount of Zn (x value) increases from 0 to 0.10, the relative density of the samples increases rapidly from 84.3% to 96.6%. And a high relative density of 95.3% is still gotten when x further increases up to 0.15. It can be seen that the YCCZ10 sample shows the maximum relative density, which indicates again that the small amount of doped Zn (10%) can effectively increase the sintering ability of $Y(Ca)CrO_3$ material. Fig. 5 shows the SEM images of the fracture surfaces of the $Y_{0.7}Ca_{0.3}Cr_{1-x}Zn_xO_{3-\delta}$ samples sintered at 1400 °C for 4 h. It can be observed that the average grain size grew up apparently as the doping amount of Zn increased from 0 to 0.15. Also, the size of pores decreased with Zn amount. It is obvious that a dense microstructure was obtained as the doping amount of Zn increased up to 0.10.

Several studies have reported that ZnO doping can effectively enhance the sintering ability of $BaZrO_3$-based materials, principally attributing this enhancement in sintering to the sintering aid function of ZnO [18–20]. Investigations on $LaCrO_3$ system have found out that chromium component has the tendency to volatilize and then deposit on the particle surface during sintering at high temperature in air, which prevents the particles from contacting each other, and from further growing. This is the main reason why it is very difficult to obtain this kind of material with dense state by sintering in air [21,22]. For the similar reason, it is hard for $YCrO_3$ material system to be densely sintered in air. As verified by the above results, Zn doping can effectively enhance the sintering of $Y(Ca)CrO_3$ material in air. This phenomenon is not only because Zn acted as sintering aid, but also the volatilization of chromium was effectively reduced for the partial substitution of Zn for Cr-site.

3.4. Electrical conductivity

Fig. 6 shows the temperature dependence of the conductivity of $Y_{0.7}Ca_{0.3}Cr_{1-x}Zn_xO_{3-\delta}$ sintered at 1400 °C for 4 h in air. The increment of electrical conductivity of zinc-doped yttrium chromites can be explained by electronic compensation mechanism [23,24], as well as the increase of the relative density of the samples. According to Fig. 6b, it can be seen that between 773 K and 1123 K, the plots of $\ln(\sigma T)$ (where σ is the electrical conductivity and T is the absolute temperature) versus $1/T$ are linear, which agrees with the following equation derived from the theory of small polaron conduction:

$$\sigma = \frac{A}{T} \exp\left(-\frac{E_a}{kT}\right) \quad (3)$$

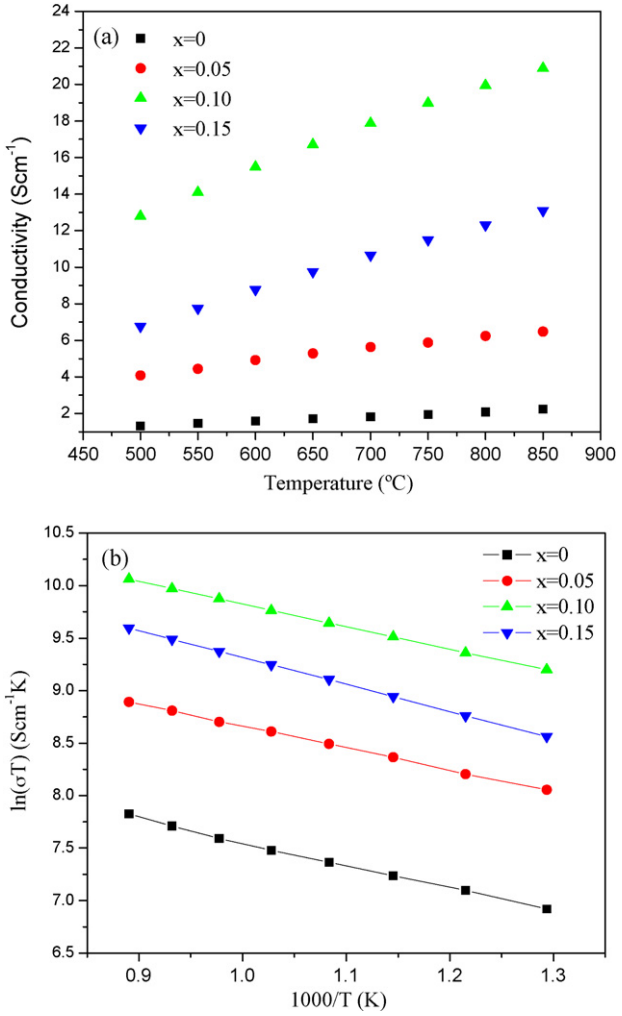

Fig. 6. Temperature dependence of the conductivity of $Y_{0.7}Ca_{0.3}Cr_{1-x}Zn_xO_{3-\delta}$ sintered at 1400 °C for 4 h: (a) effect of x value on electrical conductivity of the specimens and (b) Arrhenius plots of the conductivities for the samples.

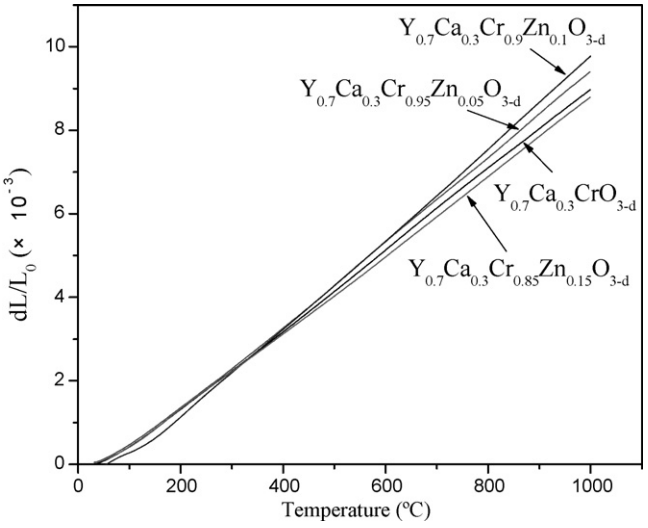

Fig. 7. Thermal expansion of $Y_{0.7}Ca_{0.3}Cr_{1-x}Zn_xO_{3-\delta}$ samples.

where A is a constant, k is the Boltzmann constant and E_a is the activation energy of conduction. The electrical transport in doped $YCrO_3$ is dominated by small-polaron hopping of charge carrier localized at the Cr-sites. It can be predicted from Eq. (2) that in the range of 0–0.1, the concentration of $Cr_{Cr}^{\bullet}$ increases with x increasing, which leads to the increase of electrical conductivity as the concentration of small polarons increases. Fig. 6a shows that the electrical conductivities of the samples sharply increase from 2.2 S cm^{-1} to a maximum of 20.9 S cm^{-1} at 850 °C in air, with Zn doping amount increasing from 0 to 0.10. However, with x further increasing up to 0.15, the electrical conductivity decreases to 13.1 S cm^{-1} at 850 °C in air. It is worthy to note that even at 500 °C, the conductivity of YCCZ10 still reaches a relatively high value of 12.8 S cm^{-1}. For a value of 1 S cm^{-1} is an acceptable minimum electrical conductivity for the usefulness of interconnects in SOFC community [25], indicating this material is suitable to be used as interconnect materials for IT-SOFCS. By calculating from the slope rate of the lines shown in Fig. 6b, the activation energy for YCCZ10 is 17.9 kJ/mol, approaching to those of $Y_{0.7}Ca_{0.3}CrO_{3-\delta}$ and $Y_{0.7}Ca_{0.3}Cr_{0.95}Zn_{0.05}O_{3-\delta}$ (Table 1), while it comes up to 21.3 kJ/mol at $x = 0.15$. Between 0.1 and 0.15 (x value), the mutation of electrical conductivity and activation energy relates to that Zn doping amount (0.15) exceeds its substitution limit for Cr position.

3.5. Thermal expansion coefficient (TEC)

The TEC of SOFC interconnects must be close to those of other cell components to minimize thermal stresses. Fig. 7 shows the thermal expansion of $Y_{0.7}Ca_{0.3}Cr_{1-x}Zn_xO_{3-\delta}$ in the temperature range of 30–1000 °C in air. The TEC values of the samples are listed in Table 1. With x increasing from 0 to 0.10, the TEC values increase from 9.6×10^{-6} to 10.8×10^{-6} K^{-1}. The TEC value of the sample decreases to 9.3×10^{-6} K^{-1} as x further increases to 0.15. This mutation may also relate to that Zn atom partially come into perovskite crystal interstitial position. It is delight to see that the TEC value of YCCZ10 (10.8×10^{-6} K^{-1}) is very close to that of the commonly used SOFC electrolyte YSZ ($\sim 10.8 \times 10^{-6}$ K^{-1}).

4. Conclusions

By employing a microwave-aided sol–gel process, $Y_{0.7}Ca_{0.3}Cr_{1-x}Zn_xO_{3-\delta}$ ($x = 0, 0.05, 0.1, 0.15$) were prepared and then investigated, and the results indicate that a small amount of Zn as dopant can effectively improve the sintering ability of the material. The compositions all showed pure orthorhombic perovskite structure. As Zn doping amount increases from 0 to 0.10, the relative density of the samples increases rapidly from 84.3% to 96.6% after sintering at 1400 °C for 4 h in air, and the electrical conductivity increases from 2.2 S cm^{-1} to 20.9 S cm^{-1} at 850 °C in air. As Zn doping amount further increases up to 0.15, the electrical conductivity remarkably drops to 13.1 S cm^{-1}, companying with a slight decrease in relative density. The TEC value of YCCZ10 is 10.8×10^{-6} K^{-1}, very close to that of YSZ. So this material is more suitable to be used as a novel interconnect material for co-fired YSZ-based SOFCs.

Acknowledgements

The authors would like to thank the financial support from Chinese Natural Science Foundation on contract No. 50572099, No. 50730002, and the financial support from the National High-tech R&D Program of China (Grant No.: 2007AA05Z157).

References

[1] N. Laosiripojana, S. Assabumrungrat, J. Power Sources 163 (2007) 943.

[2] S.C. Singhal, K. Kendall (Eds.), High-temperature Solid Oxide Fuel Cells: Fundamentals, Design and Applications, Elsevier, Oxford, UK, 2003.
[3] W.Z. Zhu, S.C. Deevi, Mater. Sci. Eng. A 348 (2003) 227.
[4] J.W. Fergus, Solid State Ionics 171 (2004) 1.
[5] N. Sakai, H. Yokokawa, T. Horita, K. Yamaji, Int. J. Appl. Ceram. Technol. 1 (2004) 23.
[6] W.J. Weber, C.W. Griffin, J. Lambert Bates, J. Am. Ceram. Soc. 70 (1987) 265.
[7] C.E. Hatchwell, N.M. Sammes, G.A. Tompsetta, I.W.M. Brown, J. Eur. Ceram. Soc. 19 (1999) 1697.
[8] S. Wang, M. Liu, Y. Dong, K. Xie, X. Liu, G. Meng, Mater. Res. Bull. 43 (2008) 2607.
[9] M. Liu, L. Zhao, D. Dong, S. Wang, J. Diwu, X. Liu, G. Meng, J. Power Sources 177 (2008) 451.
[10] X. Zhou, J. Ma, F. Deng, G. Meng, X. Liu, J. Power Sources 164 (2007) 293.
[11] R. Subasri, T. Mathews, K. Swaminathan, O.M. Sreedharan, J. Alloys Compd. 354 (2003) 193.
[12] M. Mori, H. Itoh, N. Mori, T. Abe, O. Yamamoto, Y. Takeda, N. Imanishi, Science and Technology of Zirconia, The Australia Ceramic Society, 1993, p. 776.
[13] T. Yamamoto, H. Itoh, M. Mori, N. Mori, T. Watanabe, N. Imanishi, Y. Takeda, O.O. Yamamoto, J. Power Sources 61 (1996) 219.
[14] N.Q. Minh, T. Takahashi, Science and Technology of Ceramic Fuel Cells, Elsevier, Amsterdam, 1995.
[15] I.V. Oryshich, N.E. Poryadchenko, N.D. Bega, A.N. Rakintskii, Powder Metall. Met. Ceram. 35 (1996) 3.
[16] M.M. Nasrallah, J.D. Carter, H.U. Anderson, R. Koc, in: F. Grosz, P. Zegers, O. Singhal, O. Yamamoto (Eds.), Proceedings of the 2nd International Symposium on Solid Oxide Fuel Cells, Commission of the European Communities, Luxembourg (1991) 637.
[17] T.R. Armstrong, J.W. Stevenson, D.E. McCready, S.W. Paulik, P.E. Raney, Solid State Ionics 92 (1996) 213.
[18] S.W. Tao, J.T.S. Irvine, J. Solid State Chem. 180 (2007) 3493.
[19] S.W. Tao, J.T.S. Irvine, Adv. Mater. 18 (2006) 1581.
[20] P. Babilo, S. Haile, J. Am. Ceram. Soc. 88 (2005) 2362.
[21] L. Groupp, H.U. Anderson, J. Am. Ceram. Soc. 59 (1976) 449.
[22] H. Yokokawa, N. Sakai, T. Kawada, M. Dokiya, J. Electrochem. Soc. 138 (4) (1991 1018).
[23] D.P. Karim, A.A. Aldred, Phys. Rev. B 20 (1979) 2255.
[24] M. Kertesz, I. Riess, D.S. Tannhauser, R. Langpape, F.J. Rohr, J. Solid State Chem. 42 (1982) 125.
[25] N.Q. Minh, C.R. Horne, F.S. Liu, D.M. Moffatt, P.R. Staszak, T.L. Stillwagon, J.J. VanAckeren, Proceedings of the Twenty fifth Intersociety Energy Convention Engineering Conference, vol. 13, American Institute of Chemical Engineers, New York, 1990, p. 256.